Robust Segmentation of Aerial Image Data Recorded for Landscape Ecology Studies

Rafael Guillermo Gonzalez Acuña[1]([✉]), Junli Tao[2], Daniel Breen[2],
Barbara Breen[2], Steve Pointing[2], Len Gillman[2], and Reinhard Klette[2]

[1] Centro de Investigaciones en Óptica, León, Guanajuato, Mexico
`rafael@cio.mx`
[2] Auckland University of Technology, Auckland, New Zealand

Abstract. Remote sensing from unmanned aerial vehicles provides an opportunity to bridge the gap between fine scale ground-based measurements and broad scale observations from conventional aircraft and satellites. The advantages of this approach include safe access to hazardous or difficult terrain and conditions, the ability to survey at specific times and spatial scales, and the increasingly affordable cost of this technology. These benefits have led to a rapidly expanding range of applications in natural resource management and research including mapping of terrain, vegetation cover and condition, threatened species, habitat and the impacts of agriculture, forestry, urbanisation and climate change. The analysis of these often large datasets requires reliable segmentation and classification algorithms to efficiently process information for use in landscape ecology and adaptive management. In this paper, four segmentation methods are compared using images of native vegetation, introduced weeds and agriculture recorded from a quadcopter flown over a warm temperate island (Waiheke Island, New Zealand), and also images recorded from a fixed wing UAV in a polar desert (McMudro Dry Valleys, Antarctica). We propose a post-processing method to improve the segmentation performance of the algorithms and demonstrate how this can contribute to improving research outcomes in natural resource management, conservation and agriculture.

Keywords: Image segmentation · Aerial video data · UAV · Waiheke Island · Antarctica · Performance evaluation · Segmentation measure

1 Introduction

Unmanned aerial vehicles (UAVs) were initially developed for military purposes but their potential was quickly recognised for civilian applications. Examples include [18] who proposes the use of UAVs for vineyard management based on vegetation canopy reflectance, mapping of invasive weeds [17] to plan herbicide applications, or using an infra-red camera to map the *crop water stress index* (CWSI) to guide irrigation. [2,6] use UAVs to monitor soil erosion. [21] use aerial data for quantifying tree height by reconstructing 3D clouds of points.

Vegetation classification is a an important source of information for conservation science, agriculture, forestry and planning. UAV technology provides an alternative to ground-based measurements and satellite data as a means of obtaining suitable imagery for vegetation classification. [19] uses k-means clustering to classify airborne laser scans from UAVs into two different forest regions. [7,9,15] also use UAV remote sensing to classify vegetation. [22] compares classification methods for data recorded from an UAV.

The basic intention of image segmentation is the partitioning of an image into connected regions of pixels defined by similar colour or texture. In general it is concluded in the papers cited above that segmentation-based classification methods outperform pixel-based classification methods. In this paper, we compare four segmentation algorithms using aerial data recorded with UAVs over a warm temperate island (Waiheke Island, New Zealand) or in a polar desert (McMudro Dry Valleys, Antarctica) [3]. Figure 1 shows a mosaic generated from individual frames of a video recorded in New Zealand.

The algorithms compared are *simple linear iterative algorithm* (SLIC) [1], a *Gaussian mixture model* (GMM) [13], a *hidden Markov model with expectation maximisation* (HMM-EM) [20], and a *mean-shift* (MS) algorithm [5]. We assess the performance of these algorithms in classifying native forest, agriculture and invasive weeds, and also dry valley habitats in Antarctica. However, as none of these methods performed well, we propose a post-processing technique to merge
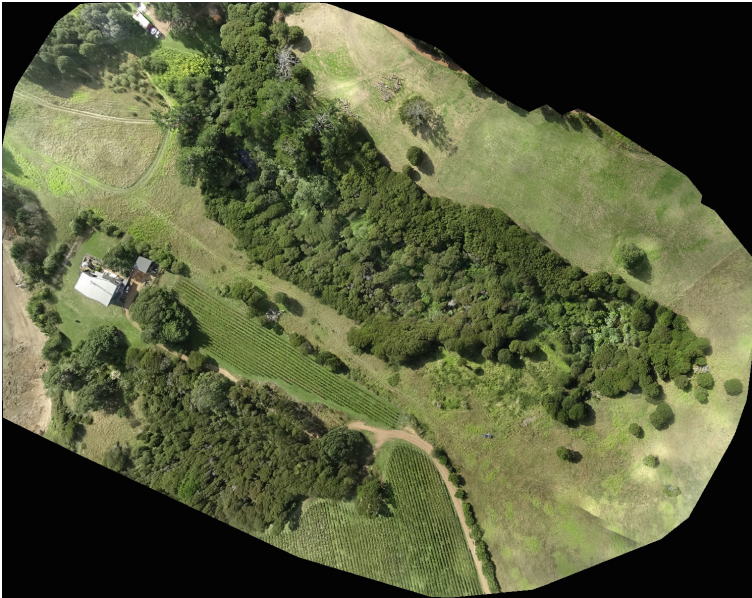
Fig. 1. Native vegetation, exotic weed species and agricultural land on Waiheke Island, Auckland, New Zealand. Mosaic processed using Pix4Dmapper Pro 2.071 from Sony Action Cam images taken from a Blade QX350 quadcopter

and split output regions to improve the classification of the original segmentation algorithms.

The segmentation step (i.e. being only an initial step in a sequence of scene analysis procedures) aims at separating the scene into semantic regions, for instance, into lawn, forest, patches of gravel, or houses. We use a colour and texture similarity measure for post-processing.

The paper is structured as follows. Section 2 presents the segmentation methods and discusses the drawbacks for our image data. In Sect. 3, the proposed post-process is reported. A comparative performance analysis is given in Sect. 4. Section 5 concludes.

2   Segmentation Methods

The trials were conducted on images from Waiheke Island, New Zealand, recorded with a Sony Action Cam HDR100 camera mounted on a Blade QX350 version 3 quadcopter UAV, and from the Taylor Dry Valleys in Antarctica recorded from a fixed wing Skycam "Polarfox" with Sony Nex5 camera (Bollard-Breen et al. 2015). The images were initially segmented using the SLIC, GMM, HMM & EM, and MS algorithms. Each method has its merits and drawbacks for tackling different image segmentation tasks.

2.1   Tested Segmentation Methods

We briefly recall those segmentation methods later used in Sect. 4. Given an $N \times N$ image I (for notational simplicity in this paper we assume square images), those four methods are applied to generate a *labelling* f (i.e. the segmentation result) which assigns uniquely a segment number (i.e. the *label*) to each of the N^2 pixels.

SLIC. SLIC is a segmentation algorithm that segments images into "nearly convex" regions called *superpixels*. It uses a strategy similar to *k-means* but with some crucial modifications. Every cluster has a defined neighbourhood, and the algorithm is spatially constrained to only merge pixels if they are near the cluster. The size of the considered neighbourhood is proportional to the number k of clusters in the image. This number k is the only input parameter for the procedure.

The clustering distance depends on the $L^\star a^\star b^\star$ colour of the pixels and their (x, y) coordinates. See [1,14] for details. Consider pixel $(x_i, y_i, L_i, a_i, b_i)$ and cluster centroid $(x_j, y_j, L_j, a_j, b_j)$. SLIC uses the following distance between both:

$$D_{SLIC} = \sqrt{d_c^2 + \frac{d_s^2}{S^2}\lambda^2}, \quad \text{where} \quad S = \sqrt{N/k} \tag{1}$$

$$d_c = \sqrt{(L_i - L_j)^2 + (a_i - a_j)^2 + (b_i - b_j)^2} \tag{2}$$

$$d_s = \sqrt{(x_i - x_j)^2 + (y_i - y_j)^2} \tag{3}$$

where d_c is the color distance, d_s the spatial distance, S is the length of one side of a *cluster neighbourhood*, and $\lambda > 0$ is a weight constant. See [1].

GMM. GMM specifies a segmentation method based on a parametric model in which the probability density function of the levels in the image is a mixture of a number of different Gaussian density functions. The goal of GMM is to find the optimal thresholds that divide the probability density function of the image (i.e. the histogram of the given image) in κ Gaussian density functions, where each Gaussian density function represents a region of the image. See [13]. The Gaussian density function has the following form:

$$\Pr(u|C_j) = \frac{1}{\sigma_j \sqrt{2\pi}} \cdot e^{-\frac{(u-\mu_j)^2}{2\sigma_j^2}} \tag{4}$$

where $\Pr(.|C_j)$ is the jth Gaussian density function for image values u; σ_j^2 is the standard deviation, and μ_j is mean value of this Gaussian density function.

HMM & EM. HMM & EM is an edge-prior preserving segmentation algorithm which can be used for obtaining accurate segmentation labels by using the maximum a posteriori (MAP) criterion. This algorithm uses an initially segmented image, which is obtained using GMM or k-means clustering with estimated parameters. See [20].

HMM & EM is defined for images $I = (\mathbf{u}_1, \ldots, \mathbf{u}_{N^2})$, drawn from an assumed distribution, where N^2 is the total number of pixels, and each $\mathbf{u}_i$ represents the values of the colours of a pixel, with $\mathbf{u}_i = [u_{iR}, u_{iG}, u_{iB}]^\top$. Let $L = \{l_1, \ldots, l_m\}$ be a set of possible labels, also drawn from an assumed distribution. See [20]. The goal of HMM & EM is to find a labeling f^* (i.e. which maps all N^2 values uniquely into set L) which satisfies

$$f^* = \operatorname{argmax}_f \{\Pr(I|L, \Theta)\Pr(L)\} \tag{5}$$

where $\Theta = \{\theta_l : l \in L\}$ is a set of distribution parameters

$$\theta_l = \{(\mu_{l,1}\sigma_{l,1}, w_{l,1}), \ldots, (\mu_{l,g}\sigma_{l,g}, w_{l,g})\} \tag{6}$$

for g Gaussian components, each having μ as mean value and σ as standard deviation; w is a weighting probability.

MS: MS is a variant of the steepest-ascent method to seek stationary peaks in a density function defined in a property space. Properties are values in the image (values directly available, such as colour values at pixels or coordinates, or values derived at pixels, such as local variance or gradient values). The algorithm is basically a density estimator. Discrete gradients are estimated in property space using a local weighting function (the *kernel*) for approximating derivatives. Let r be the radius of the kernel function K, and K' is the derivative of this kernel K.

The resulting steepest-ascent gradient defines the mean-shift vector, thus a new location in property space, where the procedure repeats, until the magnitude of the gradient is close to zero. The used density estimator has the following form:

$$E_K(\mathbf{u}) = \frac{c_k}{Mr^n} \sum_{i=1}^{M} K(\frac{1}{r^2}||\mathbf{u} - \mathbf{u}_i||_2^2) \tag{7}$$

The function is defined by kernel K at property points or vectors $\mathbf{u}$ in an n-dimensional property space, c_k is a normalization constant, M is the number of property vectors $\mathbf{u}$. For time-efficiency reasons we use a simplified MS algorithm, basically without the second (delineation) step in [5].

2.2 Drawbacks of the Segmentation Methods

The above segmentation methods have some important drawbacks for the considered application, and we discuss those here. See Figs. 2 and 4.

SLIC. SLIC has two main problems, over-classifying a single relatively homogenous region into many different superpixels, and forming large superpixels that contain two or more regions inside. The latter mostly occurs with superpixels around the borders of the image, or where there are not enough superpixels to segment the image.

GMM. GMM tends to create many isolated pixels and many *islands* (i.e. connected regions of pixels that are surrounded by pixels of another region). Borders between regions are also not well defined, and the regions intercalate gradually.

HMM & EM. HMM & EM tends to classify images into nested regions where a segment is surrounded by a larger region, which in turn lies within another larger region. This pattern does not adequately describe the patterns present in studied vegetation or landscape images.

MS. In the mean-shift segmentation, the number of clusters depends on the image and creates a very large number of labels for segments belonging to the same semantic region. This can be avoided by a post-processing algorithm to join similar regions into single segments.

3 Proposed Post-processing

Given a label map I^m generated by a segmentation method (i.e. representing a labelling function f in form of an image), we propose post-processing to improve the segmentation performance of those methods by splitting segments, merging segments, and avoiding islands. In this section, we report the proposed post-process.

Splitting Segments. We introduce color similarity to decide whether to further split segments or not. In I^m, one segment may contain multiple regions, such

as both grass and forest regions, which require further segmentation. We introduce color similarity for deciding further splitting segments or not. The splitting condition is formulated as follows:

$$\sigma_{color_i} < \tau_1 \tag{8}$$

$$\sigma_{color_i} = \sqrt{\sigma_{L_i}^2 + \sigma_{a_i}^2 + \sigma_{b_i}^2} \tag{9}$$

where i denotes the ith segment, and L, a, and b are the color components in the L*a*b* color space. σ denotes the standard deviation. If the value of the standard deviation σ_{color_i} is over the threshold τ_1, the segment i is further segmented using the SLIC method.

Algorithm 1. Splitting segments

1: **for** $i = 1$ to $N_{segments}$
2: $\sigma_{color_i} = \sqrt{\sigma_{L_i}^2 + \sigma_{a_i}^2 + \sigma_{b_i}^2}$
3: **if** $\sigma_{color_i} > \tau_1$
4: Apply SLIC to segment i
5: Update the labelling f (or map I^m) and $N_{segments}$
6: **end if**
7: **end for**

Merging Segments. As a result of the original segmentation, or after performing further splitting, a region (e.g. grass) might be segmented into too many smaller segments. We use color similarity and a texture-based measure for merging segments. The Laplacian kernel calculates an approximate of second-order derivatives along horizontal and vertical directions in an image; we compute the Laplacian in luminosity images [8,10]. Due to changes in illumination, misclassifications may occur as the texture information is illumination independent.

The merging condition is defined as follows:

$$D_{ij} < \tau_2 \tag{10}$$

$$\mathcal{L}_{ij} < \tau_3 \tag{11}$$

$$D_{ij} = \sqrt{(L_i - L_j)^2 + (a_i - a_j)^2 + (b_i - b_j)^2} \tag{12}$$

$$\mathcal{L}_{ij} = |\mathcal{L}_i - \mathcal{L}_j| \tag{13}$$

where L_i is the average value of luminosity of the segment i, L_j is the average value of the luminosity of segment j, and a_i and a_j are the average values of the a component of the segment i and j, respectively, and b_i and b_j are the average values of the b component of the segments i and j, respectively. $\mathcal{L}_i$ and $\mathcal{L}_j$ are the average values of the Laplacian of segments i or j, respectively. If the color similarity D_{ij} or texture similarity $\mathcal{L}_{ij}$ is smaller than a threshold, the two segments i and j are merged into one segment.

Algorithm 2. Merging segments

1: **for** $i = 1$ to $N_{segments}$
2: **for** $j = 1$ to $N_{segments}$
3: **if** $i = j$
4: $D_{ij} = \sqrt{(L_i - L_j)^2 + (a_i - a_j)^2 + (b_i - b_j)^2}$
5: $\mathcal{L}_{ij} = |\mathcal{L}_i - \mathcal{L}_j|$
6: **if** $D_{ij} < \tau_2 || \mathcal{L}_{ij} < \tau_3$
7: Merge segment i and segment j into one
8: Update the labelling f (or map I^m) and $N_{segments}$
9: **end if**
10: **end for**
11: **end for**

Avoiding of Islands. An island is a connected cluster of pixels that is surrounded by pixels of another segment. These islands complicate the interpretation of the resulting image, so we use a filter, sized 3×3, to remove small islands. If more than four adjacent pixels (using 8-adjacency) have the same segment label, and the label is different from the central pixel label, the central pixel label is changed to the majority label in the 8-neighborhood.

Algorithm 3. Avoiding islands

1: **for** i=2:size(Label image,1)-1
2: **for** j=2:size(Label image,2)-1
3: Take the 8-adjacent pixels that surround the current pixel: $f(i+1,j)$, $f(i-1,j)$, $f(i,j+1)$, $f(i,j-1)$, $f(i+1,j-1)$, $f(i-1,j+1)$, $f(i+1,j+1)$ and $f(i-1,j-1)$
4: Check their labels
5: Find $L_{maxfrequency}$, the label that occurs most frequently in the 8-neighborhood
6: **if** $L_{maxfrequency} > 4$ **do**
7: The current pixel is labelled by this most frequent label $f(i,j) = L_{maxfrequency}$
8: **end if**
9: **end for**
10: **end for**

## 4 Comparative Performance Analysis

The experiments are conducted on images recorded with a Sony NEX5N14Mp camera mounted on a Swampfox UAV. The test parameters for individual methods were set to $\tau_1 = 5.5$, $\tau_2 = 62$, and $\tau_3 = 2.3$ for the illustrated Waiheke video, and to $\tau_1 = 3.5$, $\tau_2 = 50$, and $\tau_3 = 0.2$ for the used Antarctica images.

The original segmentation results are shown in Fig. 2. The SLIC method generates similar-sized nearly rectangular segments and follows edges between grass and forest. GMM labels segments pixel-by-pixel which generates many small islands. The GMM segments follow outlines of interest better than SLIC

segments. The HMM-EM method generates smooth multiple-layer segments and is sensitive to regions with different colours or texture. MS generates an enormous number of islands; the results of the applied MS algorithm appear to be too sensitive to value changes.

The segmentation results with the post-processing are shown in Fig. 3. The borders between grass and forest are improved significantly. The various color and texture regions within the forest are separated to a certain level. The post-processing parameters τ can be adjusted accordingly for different applications.

The results change with the thresholds used. Here we present results for thresholds that divide the used Waiheke images into forest and grass. However, the thresholds can also be adjusted to achieve a modified segmentation for different targets, for example for groups of trees.
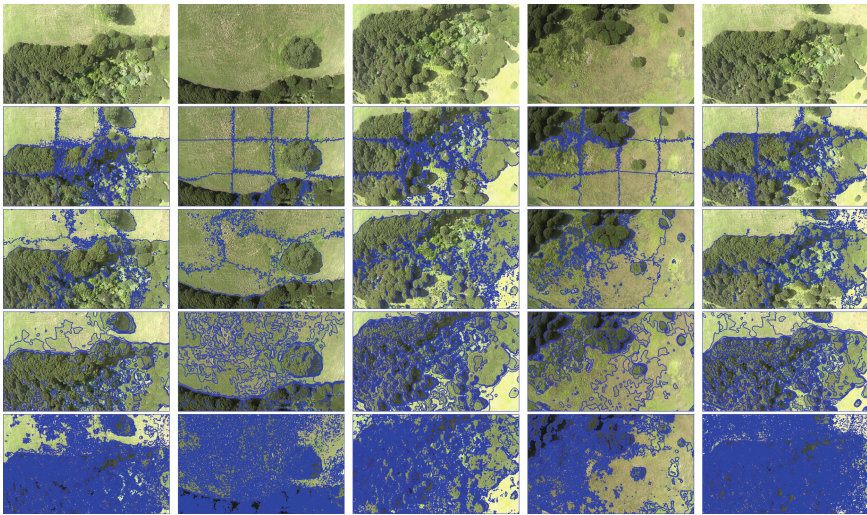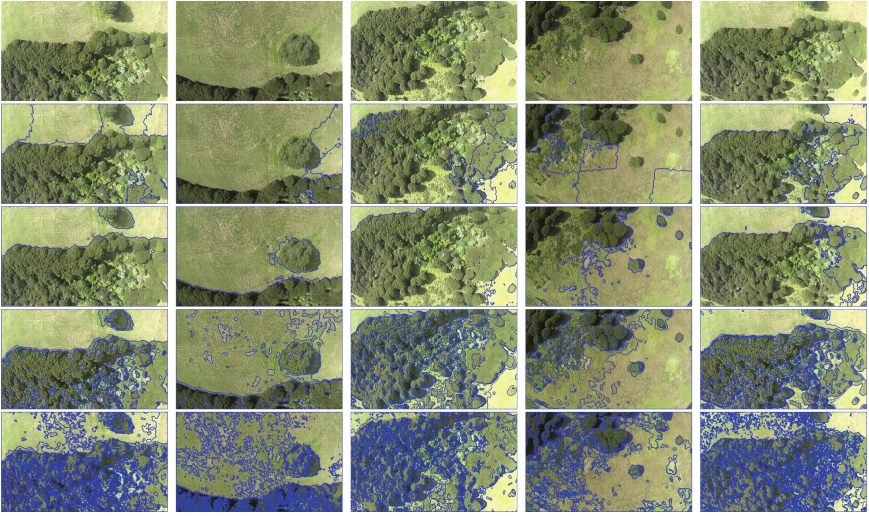

Fig. 2. Segmentation results of original segmentation methods. *Top* to *bottom*: input images, results by SLIC method, results by GMM method, results by HMM-EM method and results by MS method

Figure 4 shows results using the original segmentation techniques for two images from data base. In the first column are the images, the second column are the resulting images when SLIC is applied, the third column are the resulting GMM images, and in the last column are the images when HMM-EM is used.

In Fig. 5 we illustrate the effects of our post-process. The post-process helps to clean the results of the GMM (avoiding the islands). In the resulting GMM images, borders follow better the outlines of interest than SLIC. Also, in this case, the HMM-EM method generates smooth multiple-layer segments.
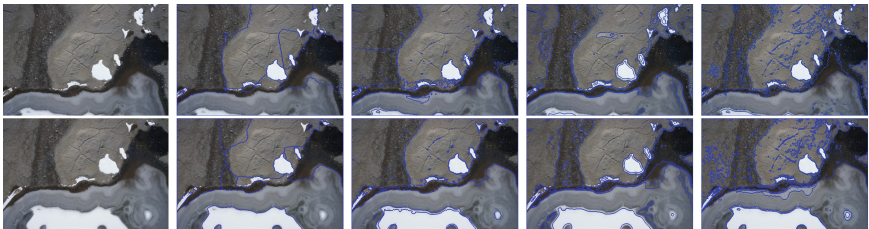
Fig. 3. Segmentation results after the proposed post-processing. *Top* to *bottom*: input images, results by SLIC method with post-processing, results by GMM method with post-processing, results by HMM-EM method with post-processing and results by MS method with post-processing
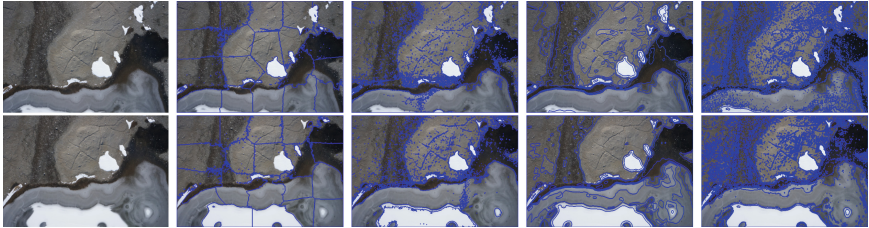
Fig. 4. Segmentation results of the Antarctica images with the original segmentation methods. *Left* to *right*: input images, results by SLIC method, results by GMM method, results by HMM-EM method and results by MS method

Fig. 5. Segmentation results of the Antarctica images when it is applied the proposed post-processing. *Left* to *right*: input images, results by SLIC method with post-processing, results by GMM method with post-processing, results by HMM-EM method with post-processing and results by MS method with post-processing

4.1   Quantitative Measurement

Let $\mathcal{S} = \{S_1, \ldots, S_{N_{segments}}\}$ be a segmentation result. We introduce a quantitative measure for $\mathcal{S}$. In this measure, segments with small standard colour deviation and larger areas are preferred. The measure is defined as follows:

$$\chi(\mathcal{S}) = \frac{1}{N_{segments}} \sum_{i=1}^{N_{segments}} \frac{A_i}{\sigma_{color_i}+1} \tag{14}$$

where i denotes segment S_i, σ_{color_i} is the standard colour deviation in S_i, $N_{segments}$ is the total number of segments, and A_i is the number of pixels in S_i, known to be a good estimator for the area of a region [11]. We identify a larger value of $\chi(\mathcal{S})$ with a *better* segmentation performance for the defined target. Results of this measure for the shown Waiheke images are listed in Tables 1 and 2. Results for the shown Antarctica images are in Table 3.

Table 1. Values $\chi(\mathcal{S})$ for the original Waiheke segmentation results

	Image 1	Image 2	Image 3	Image 4	Image 5
SLIC	204.11	276.14	163.37	288.22	181.2
GMM	296.78	390.23	241.49	391.55	261.91
HM & EM	202.41	249.78	203.62	351.72	205.23
MS	72.87	64.21	85.75	82.63	42.98

Table 2. Values $\chi(\mathcal{S})$ for the post-processed Waiheke segmentation results

	Image 1	Image 2	Image 3	Image 4	Image 5
SLIC	502.98	687.92	539.12	571.75	451.96
GMM	905.78	980.01	638.01	624.22	582.71
HM & EM	695.18	602.08	489.18	493.94	367.85
MS	133.51	128.45	166.78	242.45	143.89

Table 3. Values $\chi(\mathcal{S})$ for original and post-processed Antarctica segmentation results

	SLIC	GMM	HM & EM	MS
Image 6	269.22	325.66	319.25	212.85
Image 6, post-processed	397.18	368.78	450.31	464.58
Image 7	249.18	376.02	301.19	222.43
Image 7, post-processed	361.21	565.47	569.49	465.22

5   Conclusions

This paper compared four segmentation methods on aerial data recorded with
an UAV. Different methods have their own merits and drawbacks. SLIC gener-
ates similar sized segments. GMM produces isolated regions, and HMM & EM
generates regions with smooth borders. MS produces an enormous number of
isolated pixels, but the post process cleans the resulting images. We propose
post-processing for splitting and merging segments. The parameter settings can
be adjusted according to requirements of given applications. We also introduced
a measure for evaluating segmentation results and illustrated the measure based
on samples of video data recorded at a warm temperate island (Waiheke Island,
New Zealand), and in a polar desert (McMudro Dry Valleys, Antarctica).

In conclusion of our extensive experiments, we consider a two-step proce-
dure as being very attractive in our further studies: First, apply GMM and
post-processing for having "clean" borders between regions of interest (possibly
followed by spline approximation [4,12] for smoother borders). Second, apply
SLIC only within each region provided by the first step for identifying ecologi-
cally important smaller segments.

References

1. Achanta, R., Shaji, A., Smith, K., Lucchi, A., Fua, P., Süsstrunk, S.: SLIC super-
   pixels compared to state-of-the-art superpixel methods. IEEE Trans. Pattern Anal.
   Mach. Intell. **34**, 2274–2282 (2012)
2. Bellvert, J., Zarco-Tejada, P.J., Girona, J., Fereres, E.: Mapping crop water stress
   index in a pinot-noir vineyard: comparing ground measurements with thermal
   remote sensing imagery from an unmanned aerial vehicle. Precis. Agric. **15**, 361–
   376 (2014)
3. Bollard-Breen, B., Brooks, J.D., Jones, M.R.L., Robertson, J., Betschart, S., Kung,
   O., Cary, S.C., Lee, C.K., Pointing, S.B.: Application of an unmanned aerial vehicle
   in spatial mapping of terrestrial biology and human disturbance in the McMurdo
   Dry Valleys, East Antarctica. Polar Biol. **38**, 573–578 (2015)
4. Boor, C.: A Practical Guide to Splines. Springer, New York (1978)
5. Comaniciu, Q., Meer, P.: Mean shift: a robust approach toward feature space analy-
   sis. IEEE Trans. Pattern Anal. Mach. Intell. **24**, 603–619 (2002)
6. d'Oleire-Oltmanns, S., Marzolff, I., Peter, K.D., Ries, J.B.: Unmanned aerial vehi-
   cle (UAV) for monitoring soil erosion in Morocco. Remote Sens. **4**, 3390–3416
   (2012)
7. Dunford, R., Michel, K., Gagnage, M., Piégay, H., Trémelo, M.L.: Potential and
   constraints of unmanned aerial vehicle technology for the characterization of
   Mediterranean riparian forest. Int. J. Remote Sens. **30**, 4915–4935 (2009)
8. Gonzalez, R.C., Woods, R.E.: Digital Image Processing, 3rd edn. Prentice Hall,
   New York (2008)
9. Ishihama, F., Watabe, Y., Oguma, H.: Validation of a high resolution, remotely
   operated aerial remote sensing system for the identification of herbaceous plant
   species. Appl. Veg. Sci. **15**, 383–389 (2012)

10. Klette, R.: Concise Computer Vision. Springer, London (2014)
11. Klette, R., Rosenfeld, A.: Digital Geometry. Morgan Kaufmann, San Francisco (2004)
12. Kvasov, B.: Methods of Shape-Preserving Spline Approximation. World Scientific Pub, London (2000)
13. Lalit, G., Thotsapon, S.: Gaussian-mixture-based image segmentation algorithm. Pattern Recogn. **31**(3), 315–325 (1998)
14. MacQueen, J.B.: Some methods for classification and analysis of multivariate observations. In: Proceedings of Berkeley Symposium Mathematical Statistics Probability, pp. 281–297 (1967)
15. Mitchell, J.J., Glenn, N.F., Anderson, M.O., Hruska, R.C., Halford, A., Baun, C., Nydegger, N.: Unmanned aerial vehicle hyperspectral remote sensing for dryland vegetation monitoring, signal processing. In: Proceedings of Workshop Hyperspectral Image, pp. 1–10 (2012)
16. Otsu, N.: A threshold selection method from gray-level histograms. IEEE Trans. Syst. Man Cybern. **9**, 62–66 (1979)
17. Peña, J.M., Torres-Sánchez, J., de Castro, A.I., Kelly, M., López-Granados, F.: Weed mapping in early-season maize fields using object-based analysis of unmanned aerial vehicle (UAV) images. PLoS ONE **8**, e77151 (2013)
18. Primicerio, J., Di Gennaro, S.F., Fiorillo, E., Genesio, L., Lugato, E., Matese, A., Vaccari, F.P.: A flexible unmanned aerial vehicle for precision agriculture. Precis. Agric. **13**, 517–523 (2012)
19. Vehmas, M., Eerikäinen, K., Peuhkurinen, J., Packalén, P., Maltamo, M.: Airborne laser scanning for the site type identification of mature boreal forest stands. Remote Sens. **3**, 100–116 (2011)
20. Wang, Q.: HMRF-EM-image: Implementation of the hidden Markov random model and its expectation-maximization algorithm (2012). arxiv: 1207.3510 [cs.CV]
21. Zarco-Tejada, P.J., Diaz-Varela, R., Angileri, V., Loudjani, P.: Tree height quantification using very high resolution imagery acquired from an unmanned aerial vehicle (UAV) and automatic 3D photo-reconstruction methods. Eur. J. Agron. **55**, 89–99 (2014)
22. Zhang, Z.: Native vegetation classification using remote sensing techniques: A case study of dairy flat regrowth bush by using the AUT Unmanned Aerial Vehicle. Doctoral dissertation. University of Technology, Auckland (2014)